Photoacoustics 50 (2026) 100843

Contents lists available at ScienceDirect

Photoacoustics

journal homepage: www.elsevier.com/locate/pacs

Nonlinear dual-frequency modulation QEPAS using a single laser for resolving overlapping spectral features

Xiaowen Shen [a,b,c,1], Lei Yang [d,1], Chaofeng Sun [a,b,1], Yan Gao [d], Marilena Giglio [a,c], Angelo Sampaolo [a,c], Pietro Patimisco [a,c], Vincenzo Spagnolo [a,c,*], Lei Dong [a,b,*], Hongpeng Wu [a,b,*]

[a] State Key Laboratory of Quantum Optics Technologies and Devices, Institute of Laser Spectroscopy, Shanxi University, Taiyuan 030006, PR China
[b] Collaborative Innovation Center of Extreme Optics, Shanxi University, Taiyuan 030006, PR China
[c] PolySense Lab-Dipartimento Interateneo di Fisica, University and Politecnico of Bari, Via Amendola 173, Bari, Italy
[d] School of Physical and Electronic Sciences, Shanxi Datong University, Datong 037009, PR China

ARTICLE INFO

Keywords:
QEPAS
Dual-frequency modulation
Non-linear competition effects
Trace gas detection

ABSTRACT

Conventional single-frequency wavelength modulation spectroscopy faces inherent limitations in multi-component gas sensing, due to restricted detection dimensionality and unavoidable trade-offs in modulation parameters. To overcome these issues, we propose a Quartz-Enhanced Photoacoustic Spectroscopy sensing technique based on single-laser dual-frequency superimposed modulation. By simultaneously injecting two independent high-frequency modulation signals, matching the fundamental and overtone resonance modes of a Quartz Tuning Fork(QTF), into a single Distributed Feedback laser, dual-channel real time synchronous detection is achieved within a compact single path optical architecture. A comprehensive physical model incorporating both Residual Amplitude Modulation and high order non-linear competition effects has been proposed. We demonstrate that the fourth derivative of the gas absorption line shape plays a dominant role in inducing signal suppression and waveform splitting under strong dual-frequency modulation. A waveform optimization strategy based on dynamically tuning the laser scanning rate allow to regulate the effective filtering behavior of the lock-in amplifier.

1. Introduction

Tunable Diode Laser Absorption Spectroscopy (TDLAS) and Quartz-Enhanced Photoacoustic Spectroscopy (QEPAS) are widely recognized as leading techniques for trace gas sensing across diverse applications, including environmental monitoring [1–6], industrial process control [7–10], medical diagnostics [11–15], and isotope analysis [16–23]. These methods offer outstanding selectivity, high sensitivity, and real-time detection capabilities. In systems based on Wavelength Modulation Spectroscopy (WMS) [24,25], the signal modulation and demodulation schemes play a critical role in determining detection limit and overall system robustness.

In QEPAS, conventional single-frequency modulation typically employs a sinusoidal drive applied to the laser, extracting the second harmonic ($2f$) signal via a lock-in amplifier to effectively suppress $1/f$ noise and subtract the background baseline [26]. This approach performs exceptionally well for isolated absorption lines and has become the standard technique in practical implementations. However, as the requirements for trace gas sensing become increasingly complex, single frequency modulation faces fundamental limitations. Simultaneous detection of multi-component gas mixtures, high precision isotope ratio analysis, and environments with significant spectral overlap impose conflicting requirements on modulation parameters, such as modulation depth and frequency response, making optimal tuning difficult. Furthermore, conventional approaches to accessing multiple spectral features often rely on time division scanning [27–30], multi-laser configurations [31–35] or multiple QTFs[36]. These strategies compromise real-time performance and substantially increase system size, optical alignment complexity, and overall hardware cost, thereby limiting their applicability in compact and portable sensing platforms.

* Corresponding authors at: State Key Laboratory of Quantum Optics Technologies and Devices, Institute of Laser Spectroscopy, Shanxi University, Taiyuan 030006, PR China.
E-mail addresses: vincenzoluigi.spagnolo@poliba.it (V. Spagnolo), donglei@sxu.edu.cn (L. Dong), wuhp@sxu.edu.cn (H. Wu).
[1] These authors contributed equally to this work.

https://doi.org/10.1016/j.pacs.2026.100843
Received 15 April 2026; Received in revised form 19 May 2026; Accepted 26 May 2026
Available online 30 May 2026

To overcome these limitations, multi-frequency modulation strategies have attracted increasing attention in recent years. Introducing an additional modulation frequency enables access to richer spectral feature information, thereby enhancing detection selectivity and improving resistance to interference. For instance, Dual-Frequency Heterodyne QEPAS (DFH-QEPAS) [37] exploits the beat frequency generated by two modulation components to drive the QTF, resulting in enhanced sensor response and sensitivity. However, most existing multi-frequency implementations rely on multi-laser configurations or complex time-division scanning schemes. These approaches inherently compromise real-time performance and introduce additional optical noise and system instability due to beam-combining optics, significantly increasing system complexity, size, and power consumption. As a result, their applicability in compact and portable sensing platforms remains limited. Although recent studies have explored electrical multi-frequency excitation using a single-laser system [38,39], these approaches are often treated within a simplified linear superposition framework. Such treatments neglect the intrinsic non-linear interactions between the modulated semiconductor laser output and the gas absorption line shape under deep modulation conditions, which can lead to significant waveform distortion and signal degradation.

To address these fundamental limitations and the critical gap in understanding non-linear dynamics, this work proposes a gas sensing technique based on single-laser dual-frequency superimposed modulation, supported by a rigorous physical model. Two high-frequency sinusoidal signals drive a single Distributed Feedback Laser (DFB) matched to the fundamental and overtone resonance modes of a QTF, enabling simultaneous dual-channel second-harmonic (2 *f*) signal extraction via orthogonal demodulation. This approach allows data acquisition in two independent detection channels within a single laser tuning cycle, preserving the intrinsic zero-background advantage of QEPAS while extending the detection dimensionality through frequency-domain separation.

The present study primarily focuses on the physical modeling and experimental validation of nonlinear competition effects in dual-frequency QEPAS, providing the mechanistic basis for future system-level implementations and multicomponent sensing applications. Beyond the modulation architecture itself, this work moves beyond conventional linear superposition assumptions by establishing a comprehensive theoretical framework incorporating both Residual Amplitude Modulation (RAM) and high-order nonlinear interaction effects. As detailed in Section 2, the model demonstrates that the intrinsic nonlinear characteristics of the gas absorption line shape give rise to inter-channel crosstalk, signal suppression, and waveform distortion under strong dual-frequency modulation conditions. These theoretical predictions are systematically validated through the experimental investigations presented in Section 3. The results demonstrate that the proposed approach not only resolves complex nonlinear waveform features, but also enables controlled suppression of distortion effects through appropriate optimization of modulation and scanning parameters. Collectively, these findings establish dual-frequency modulation as a robust strategy for extending the information content, sensitivity, and operational flexibility of QEPAS-based gas sensing systems, particularly in scenarios involving overlapping spectral features and complex spectral interference.

2. Theoretical model of dual-frequency QEPAS

2.1. Dual-frequency modulation model of laser output characteristics

In the single-laser dual-frequency detection system developed in this work, the injection current of the DFB laser is formed by superimposing a low frequency scanning sawtooth wave and two high frequency sinusoidal modulation components. The two modulation frequencies are denoted as f_1 and f_2 (with corresponding angular frequencies ω_1 and ω_2), where f_1 is matched to the fundamental resonance mode of the QTF, and f_2 to its first overtone mode. The injection current can be expressed as:

$$I(t) = I_{scan}(t) + I_1\cos(\omega_1 t) + I_2\cos(\omega_2 t) \tag{1}$$

Where $I(t)$ is the total instantaneous injection current of the laser, $I_{scan}(t)$ represents the low-frequency sawtooth wave current used for wavelength scanning, and I_1 and I_2 are the amplitudes of the high-frequency sinusoidal modulation currents at frequencies f_1 and f_2. Due to the intrinsic properties of semiconductor lasers, modulation of the injection current induces simultaneous variations in both emission frequency (wavelength) and the output optical intensity. The instantaneous laser frequency $\nu(t)$ fluctuates around the slowly varying central frequency $\nu_0(t)$, determined by the scanning signal, and can be written as:

$$\nu(t) = \nu_0(t) + \delta\nu(t) = \nu_0(t) + \Delta\nu_1\cos(\omega_1 t) + \Delta\nu_2\cos(\omega_2 t) \tag{2}$$

$\Delta\nu_1$and $\Delta\nu_2$ represent the wavenumber variation amplitudes associated with the two modulation frequencies, respectively. In addition, RAM leads to a concurrent modulation of the optical intensity. The instantaneous optical intensity $P(t)$ can be described as:

$$P(t) = P_0[1 + m_1\cos(\omega_1 t + \psi_1) + m_2\cos(\omega_2 t + \psi_2)] \tag{3}$$

Where P_0 is the average optical intensity, m_i denotes the optical intensity modulation index at the *i-th* frequency, and ψ_i represents the phase delay of intensity modulation relative to frequency modulation (FM-AM phase shift).

2.2. Gas absorption and photoacoustic signal generation mechanism

When the modulated laser beam interacts with the target gas, the absorption coefficient $\alpha(\nu)$can be expanded around the central frequency ν_0 using a Taylor series under the weak absorption approximation of the Beer–Lambert law. To accurately capture the frequency competition and non-linear crosstalk effects arising under dual-frequency modulation, the conventional second-order approximation is insufficient. Therefore, the absorption coefficient is expanded up to the fourth order:

$$\alpha(\nu) = \alpha(\nu_0) + \alpha'\delta\nu + \frac{1}{2}\alpha''(\delta\nu)^2 + \frac{1}{6}\alpha'''(\delta\nu)^3 + \frac{1}{24}\alpha^{(4)}(\delta\nu)^4 \tag{4}$$

Where $\alpha(\nu_0)$ is the absorption coefficient at the central frequency. α', α'', α''', and $\alpha^{(4)}$ represent the first, second, third, and fourth derivatives, and $\delta\nu$ denotes the frequency variation defined in Eq. (2). The thermal power density generated by the photoacoustic effect is proportional to the product of the instantaneous optical intensity and the absorption coefficient, i.e., $H(t) \propto P(t) \bullet \alpha(\nu)$ [40]. In the following analysis, we focus on the signal composition of the fundamental detection channel, demodulated at frequency f_1. By substituting Eqs. (2) and (3) into Eq. (4) and applying trigonometric identities, a term-by-term derivation can be performed. First, we analyze the main signal term generated by wavelength modulation. This term primarily originates from the product of the second-order term in Eq. (4) and the optical intensity P_0. Expanding $\delta\nu$ and taking its square yields:

$$(\delta\nu)^2 = [\Delta\nu_1\cos(\omega_1 t) + \Delta\nu_2\cos(\omega_2 t)]^2$$

$$= \Delta\nu_1^2\cos(\omega_1 t)^2 + 2\Delta\nu_1\cos(\omega_1 t) \bullet \Delta\nu_2\cos(\omega_2 t) + \Delta\nu_2^2\cos(\omega_2 t)^2 \tag{5}$$

Using the power-reduction identity $\cos^2\theta = \frac{1+\cos 2\theta}{2}$, the component at frequency $2\omega_1$ can be extracted as $\frac{1}{2}\Delta\nu_1^2\cos(2\omega_1 t)$. Substituting the second-order coefficient, the main signal amplitude is obtained:

$$S_{\text{main}} \propto \frac{1}{4}P_0\alpha''(\nu_0)\Delta\nu_1^2 \tag{6}$$

Next, we consider the distortion term introduced by the RAM effect. This term originates from the coupling between the first-order intensity

modulation term and the first derivative term of the absorption coefficient, i.e., $[P_0 m_1 \cos(\omega_1 t + \psi_1)] \bullet [\alpha' \Delta\nu_1 \cos(\omega_1 t)]$. Applying the product-to-sum identity $\cos A \cos B = \frac{1}{2}[\cos(A+B) + \cos(A-B)]$, the component at $2\omega_1$ is:

$$S_{\mathrm{RAM}} \propto \frac{1}{2} P_0 m_1 \Delta\nu_1 \alpha'(\nu_0) \cos(\psi_1) \tag{7}$$

Since $\alpha'(\nu_0)$ is an odd function with respect to the central frequency, while the main signal $\alpha''(\nu_0)$ is an even function, the superposition of this term directly introduces asymmetry in the measured waveform at the absorption peak center. Finally, we analyze the dual-frequency competition effect term. This is the key non-linear mechanism revealed in this study, originating from the cross-modulation component in the fourth derivative term $(\delta\nu)^4$. The binomial expansion on $(\delta\nu)^4$ contains the cross term $6[\Delta\nu_1 \cos(\omega_1 t)]^2 [\Delta\nu_2 \cos(\omega_2 t)]^2$. Using the power-reduction identity, this term simplifies to $\frac{3}{2}\Delta\nu_1^2 \Delta\nu_2^2 [1 + \cos(2\omega_1 t)][1 + \cos(2\omega_2 t]$. The component at $2\omega_1$ is therefore $\frac{3}{2}\Delta\nu_1^2 \Delta\nu_2^2 \cos(2\omega_1 t)$. Substituting the fourth-order coefficient $\frac{1}{24} P_0 \alpha^{(4)}$, the competition term expression is obtained:

$$S_{\mathrm{Comp}} \propto \frac{1}{16} P_0 \alpha^{(4)}(\nu_0) \Delta\nu_1^2 \Delta\nu_2^2 \tag{8}$$

According to Eqs. (6) - (8), the complete second harmonic signal expression for the fundamental detection channel is:

$$S_{2f_1} \propto P_0 [\frac{1}{4}\alpha''(\nu_0)\Delta\nu_1^2 + \frac{1}{2} m_1 \Delta\nu_1 \alpha'(\nu_0)\cos(\psi_1) + \frac{1}{16}\alpha^{(4)}(\nu_0)\Delta\nu_1^2\Delta\nu_2^2] \tag{9}$$

At the center of the absorption peak of a Lorentzian line shape, the fourth derivative $\alpha^{(4)}$ is positive, while the *2nd* derivative α'' is negative. This implies that the third term (competition term) in Eq. (9) has the opposite sign to the first term (main signal), indicating that increasing the overtone modulation depth leads to attenuation of the fundamental signal amplitude. Similarly, the complete second-harmonic signal expression for the overtone detection channel can be written as:

$$S_{2f_2} \propto P_0 [\frac{1}{4}\alpha''(\nu_0)\Delta\nu_2^2 + \frac{1}{2} m_2 \Delta\nu_2 \alpha'(\nu_0)\cos(\psi_2) + \frac{1}{16}\alpha^{(4)}(\nu_0)\Delta\nu_1^2\Delta\nu_2^2] \tag{10}$$

2.3. Low-pass filtering response under dynamic scanning

The above derivation is based on a quasi-static approximation. However, in practical operations, the laser central wavenumber $\nu_0(t)$ is typically scanned linearly in time to enable rapid spectra acquisition, i.e., $\nu_0(t) = \nu_{\mathrm{start}} + rt$, where r (cm^{-1}/s) denotes the scanning rate. Under these dynamic conditions, the integration time constant τ of the lock-in amplifier (LIA) introduces a non-negligible low-pass filtering effect. As a result, the measured output signal $S_{\mathrm{out}}(t)$ of the system can be described as the convolution of the instantaneous second-harmonic signal $S_{2f_1}(t)$ with the impulse response $h(t) = \frac{1}{\tau} e^{-t/\tau}$ of the LIA low-pass filter, given by $h(t) = \frac{1}{\tau} e^{-t/\tau}$:

$$S_{\mathrm{out}} = S_{2f_1}(t) \bullet h(t) = \int_{-\infty}^{t} S_{2f_1}(\nu_{\mathrm{start}} + r\xi) \bullet \frac{1}{\tau} e^{-(t-\xi)/\tau} d\xi \tag{11}$$

ξ is the dummy variable of integration for the convolution process. From a signal-processing perspective, the scanning rate r establishes a mapping between the spectral (spatial) frequency k and the temporal frequency ω, such that $\omega = rk$. High-order derivatives of the absorption profile correspond to higher spatial frequency components; in particular, the fourth derivative $\alpha^{(4)}$ captures fine spectral features, such as peak splitting or central dips, and therefore contains significantly higher frequency components than the second-order term α''. As the scanning rate r increases, these high-frequency components are shifted beyond the effective bandwidth of the LIA and are preferentially attenuated by its low-pass filtering characteristic. Consequently, the distortion induced by the non-linear competition term S_{comp} is progressively suppressed. This model not only explains the reduction in overall signal amplitude at high scanning rates, but also provides a physical interpretation of the experimentally observed smoothing of waveform distortions caused by high-order non-linear effects.

3. Experimental verification of the dual-modulation gas detection platform

3.1. Frequency response characterization of QTF

Characterization of the QTF frequency response is a critical prerequisite for implementing the dual-frequency photoacoustic detection system. Accurate determination of the resonant frequencies and quality factors (Q-factors) of both the fundamental and overtone modes is essential, as these parameters define the optimal laser modulation frequencies (f_1 and f_2) and directly impact the sensor sensitivity. Fig. 1 presents the results of the electrical frequency sweep of the QTF. For the fundamental mode, the resonant frequency was measured at f_1 = 2883.72 Hz. Lorentzian fit yielded a bandwidth of ~ 0.47 Hz, corresponding to a quality factor of $Q_{f1} \approx 6100$. For the first overtone mode, the resonant frequency was identified at f_2 = 17839.38 Hz, with a bandwidth of ~ 1.17 Hz and a quality factor of $Q_{f2} \approx 15250$.

In subsequent dual-frequency experiments, the laser modulation frequencies were precisely tuned to these resonance values (f_1 and f_2) to ensure operation under optimal acoustic excitation conditions. These frequencies also served as reference signals for the dual-channel lock-in amplifiers, enabling synchronized demodulation of the fundamental and overtone responses.

3.2. Construction of the dual-modulation gas detection platform

To validate the proposed dual-modulation architecture, water vapor (H_2O) was selected as the target gas due to its atmospheric abundance and well defined absorption features. The schematic of the experimental setup is illustrated in Fig. 2.

The experimental system is based on a DFB (Laser 1), whose temperature and injection current are controlled by a low-noise driver. A composite modulation signal, consisting of a low frequency sawtooth wave superimposed with two high-frequency sinusoidal components, was applied to the laser controller. This configuration enables simultaneous modulation at the fundamental f_1 and first overtone f_2 resonance frequencies of the QTF. The modulated laser beam was collimated and tightly focused between the prongs of a custom QTF to generate photoacoustic excitation. The QTF was housed in a gas cell sealed with CaF_2 windows to minimize optical insertion loss. Gas flow and pressure within the cell were precisely controlled using a mass flow controller (Alicat Scientific, M−500SCCM-D) and a vacuum pump (KNF

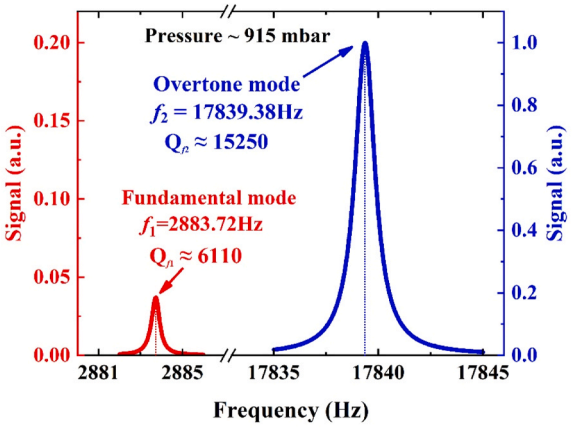

Fig. 1. Fundamental (f_1) and overtone frequency (f_2) resonance spectra.

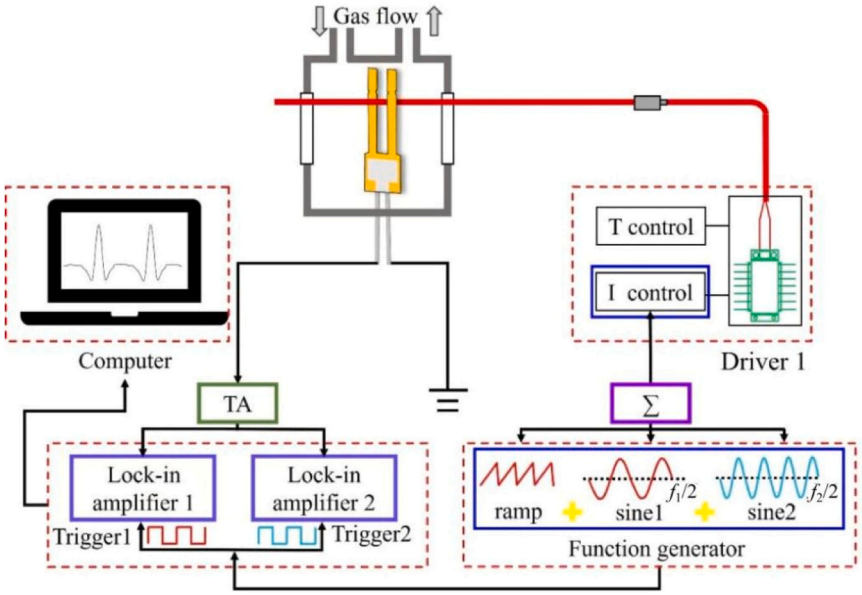

Fig. 2. Dual-modulation gas detection platform system.

Technologies, N816.3KT.18), ensuring stable measurement conditions. The laser was operated at a stabilized temperature of 22 °C and an injection current of 98.5 mA, corresponding to emission at 1368.6 nm (7306.75 cm^{-1}), targeting a strong H_2O absorption line with an output power of 8.8 mW. The piezoelectric current generated by the QTF was converted into a voltage signal via a custom transimpedance amplifier (TA) and subsequently demodulated by two LIAs (Stanford Research Systems, SR830). The LIAs were referenced to f_1 and f_2, respectively, enabling simultaneous dual-channel second harmonic (2 f) detection. For both channels, the filter slope was set to 12 dB/oct with a 1 s integration time constant. The demodulated signals were recorded and processed by a computer for real-time concentration retrieval.

Numerical simulations were first performed to predict the temporal evolution of the laser wavelength under different modulation schemes. Fig. 3(a) and (b) compare the resulting modulation profiles: the single frequency case presents a regular sinusoidal structure, whereas the dual-

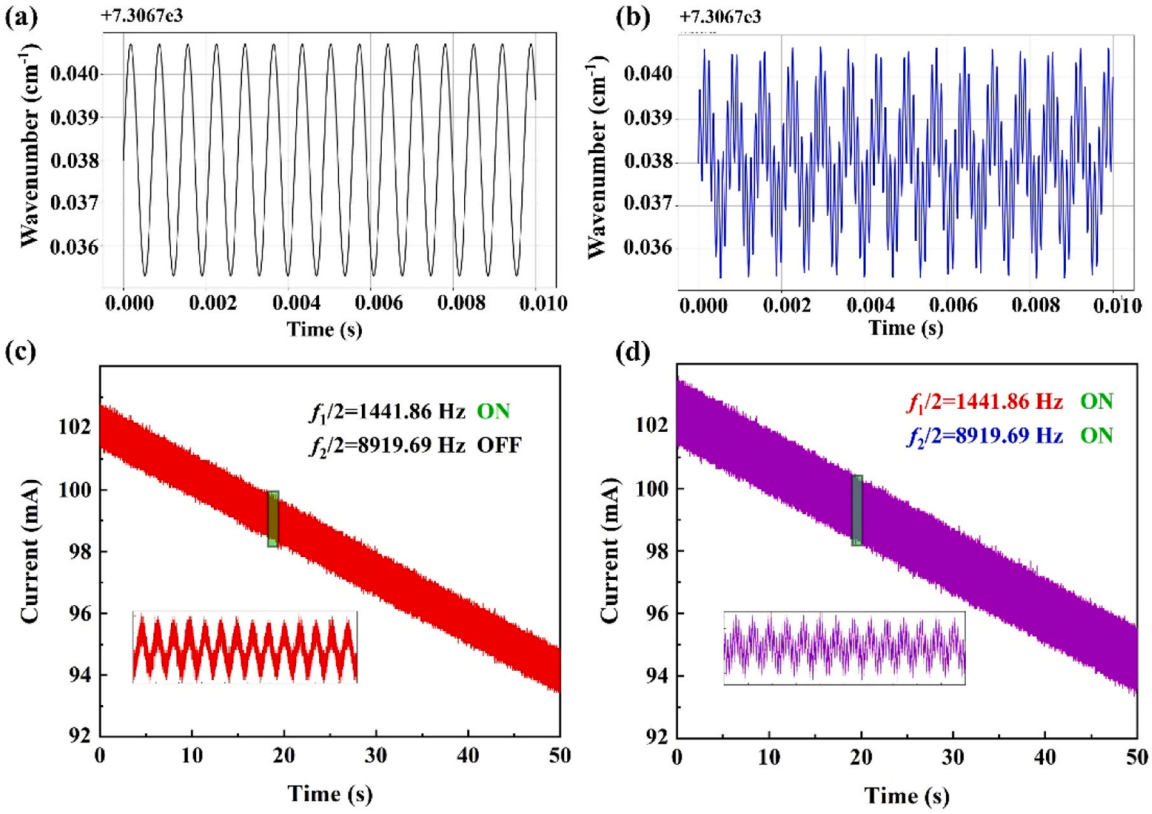

Fig. 3. Waveform simulation (Python) and experimental measurement results for traditional wavelength modulation and dual-modulation modes. (a) Simulated and (c) measured waveforms for traditional wavelength modulation mode; (b) Simulated and (d) measured waveforms for dual-modulation mode.

frequency mode produces a more complex composite waveform, arising from the superposition of two harmonic components onto the scanning trajectory.

For experimental implementation, a high precision digital synthesis approach was employed. A 20 mHz sawtooth scanning ramp was combined with the modulation carriers, either a single sinusoidal component ($f_1/2$) or a dual-frequency combination ($f_1/2$ and $f_2/2$), and generated using a Digital-to-Analog Converter (DAC). The experimentally measured tuning curves align closely with the simulation results. Specifically, the dual-frequency configuration (Fig. 3(c)) exhibits a dense oscillation pattern consistent with theoretical predictions. The magnified view in Fig. 3(d) further confirms the high fidelity of the generated waveform, with no observable phase distortion or amplitude degradation.

In contrast to conventional wavelength modulation, the dual-frequency modulation scheme applies a composite excitation signal to the laser, which alters the emission dynamics and consequently affects the spatial distribution of the generated photoacoustic signal. As a result, precise optimization of the laser beam position within the QTF prong region becomes critical. Fig. 4(b) shows the variation of the signal amplitude as the laser beam is vertically scanned along the QTF prongs. Under dual-modulation conditions, the fundamental mode exhibits a relatively uniform spatial response with minimal amplitude variation. In contrast, the overtone mode displays a pronounced spatial dependence, characterized by a decrease–increase–decrease trend. This behavior is attributed to the phase variations arising from the relative position of the acoustic excitation source with respect to the mode shape of the QTF.

To accommodate the distinct spatial characteristics of the two eigenmodes, a compromise operating point was selected by fixing the laser focus at a height of ~ 9.0 mm. This position ensures sufficient acoustic excitation of the overtone mode while maintaining stable response in the fundamental mode. Notably, the experimental results obtained at this configuration demonstrate clean signal profiles, confirming the system's ability to suppress intermodulation artifacts (e.g., $f_1 \pm f_2$) and to achieve high-fidelity, independent demodulation of the dual-channel signals.

3.3. Signal characteristic analysis under single-frequency modulation

To validate the theoretical description of RAM, specifically the contributions outlined in Eqs. 9 and 10, we first optimized the laser modulation depth under conventional single-frequency WMS operation. As shown in Fig. 5, the signal amplitude increases linearly with modulation depth before reaching a saturation point. The optimization results reveal different optimal modulation conditions for the two modes: the fundamental signal is maximal at a modulation depth of 9 mV, whereas the overtone signal peaks at 12 mV. These optimized parameters were subsequently used to acquire representative second-harmonic ($2f$) waveforms for both detection channels.

As shown in Fig. 6, the experimentally observed waveforms exhibit the expected second harmonic profile; however, they deviate from perfect even symmetry, displaying noticeable asymmetry between the left and right sides. The quantified asymmetry is approximately 3.7% for the fundamental signal and 0.07% for the overtone signal. This behavior is consistent with the theoretical model. Specifically, the first-harmonic component associated with the laser intensity modulation introduces a contribution proportional to the first derivative term of the absorption coefficient (α', odd function). This term breaks the intrinsic symmetry of the ideal second-derivative signal (α", even function). Consequently, as the modulation depth increases, the relative contribution of the RAM term becomes more significant, leading to progressively enhanced waveform asymmetry and distortion.

3.4. Analysis of signal non-linear competition effect under dual-frequency modulation

A central prediction of the proposed theoretical model is the non-linear competition effect between the dual-frequency modulation components, described by the interaction terms in Eqs. 9 and 10. The analysis indicates that increasing the modulation depth of one frequency introduces a fourth derivative contribution with a sign opposite to the primary second-order signal, leading to overall signal amplitude attenuation.

Fig. 7 presents the signal response under equal dual-frequency modulation depths ($m_1 = m_2$). The amplitude increases linearly only at low modulation current; however, once the modulation current exceeds approximately 6 mA, the $2f$ signal amplitude as a function of modulation current under dual-frequency excitation with equal amplitudes shows deviation from linear behavior at high modulation levels. The signal exhibits clear attenuation accompanied by pronounced waveform distortion, providing direct experimental evidence of strong non-linear inter-channel coupling under deep modulation conditions.

To isolate the dual-frequency interaction mechanism, a controlled parametric study was conducted by fixing the modulation depth of one channel while systematically varying the other. As shown in Fig. 8, when the fundamental modulation amplitude is fixed at 4 mV, increasing the overtone modulation amplitude leads to a pronounced modification of the fundamental-channel second-harmonic ($2f$) waveform. In addition to a clear reduction in signal amplitude, the waveform progressively develops a central dip and eventually exhibits peak splitting.

The fundamental signal includes a negative "competition term" proportional to the cross-modulation product, originating from the fourth derivative of the absorption line shape. As the overtone modulation depth increases, this fourth-order non-linear component strengthens and counteracts the primary signal associated with the

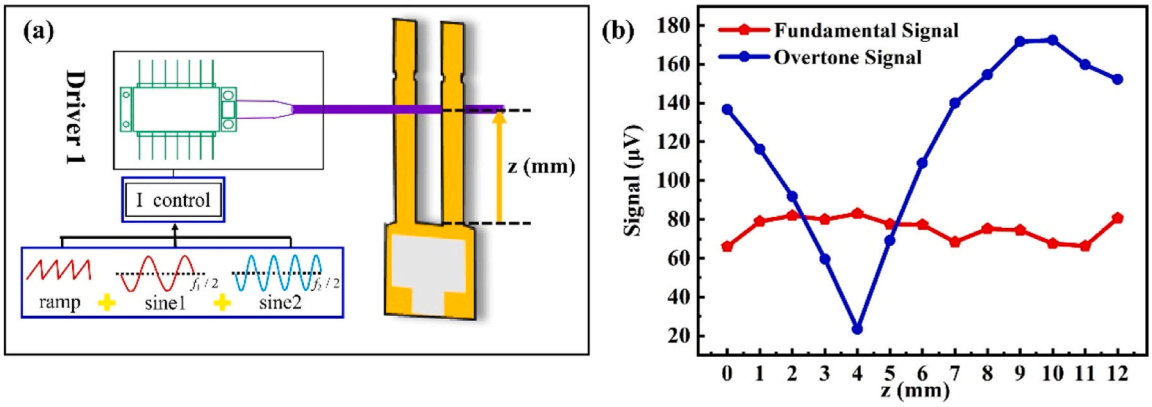

Fig. 4. Optimization of the laser beam focusing position under dual-frequency modulation. (a) schematic diagram of the vertical focusing position z along the QTF prong (b) measured fundamental and overtone signal amplitudes as a function of z.

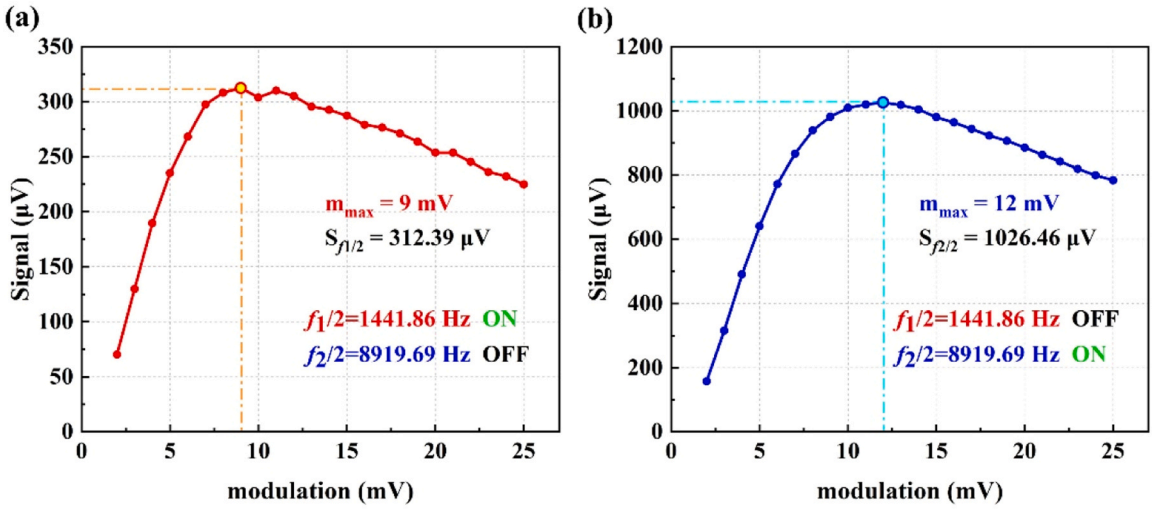

Fig. 5. Signal amplitude as a function of modulation depth under single-frequency excitation: (a) fundamental channel and (b) overtone channel.

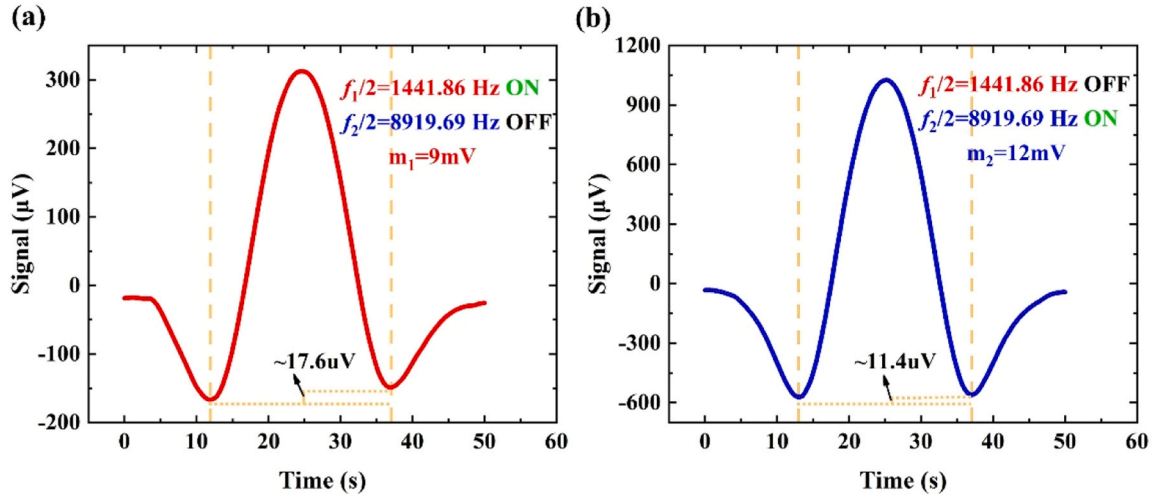

Fig. 6. 2 f signal waveforms at optimal modulation depth. (a) Fundamental 2 f waveform at $m_1 = 9$ mV. (b) Overtone 2 f waveform at $m_2 = 12$ mV.

second derivative α". This behavior demonstrates that in single-laser dual-frequency systems, frequency-domain orthogonality does not eliminate coupling at the physical level; instead, strong inter-channel interaction arises from the intrinsic non-linearity of the absorption process. The experimentally observed peak splitting indicates the onset of an over-modulation regime, in which higher-order derivative terms (e.g., fourth- and sixth-order) dominate over the second-order contribution. As illustrated in the magnified view of Fig. 8(a), increasing the overtone modulation depth from 4 to 25 mV progressively widens the peak separation, directly reflecting signal cancellation at the waveform center. In addition, the persistent left-right asymmetry observed in all waveforms further confirms the presence of RAM, consistent with the theoretical prediction in Eqs. (9) and (10).

To verify the reciprocal nature of the non-linear competition effect, the control parameters were reversed: the overtone modulation amplitude was fixed at 4 mV, while the fundamental modulation depth was systematically varied from 4 mV to 25 mV. The results, shown in Fig. 9, exhibit a trend consistent with that observed in Fig. 8. As the fundamental modulation depth increases, the overtone signal undergoes analogous degradation, characterized by amplitude attenuation, the emergence of a central dip, and eventual peak splitting. This symmetric behavior confirms the bidirectional coupling between the two modulation components and further validates the proposed non-linear interaction mechanism.

However, Figs. 7–9 represent only one-dimensional cross-sections obtained by varying a single modulation depth at a time, and therefore cannot fully describe the global coupling dynamics of the dual-frequency system. To provide a more comprehensive analysis, Fig. 10 introduces a two-dimensional parametric mapping in which the signal response is represented as a joint function of both modulation depths, m_1 and m_2.

As illustrated in Fig. 10, synchronously increasing the modulation amplitudes of both channels initially enhances the signal strength, followed by a rapid transition into a pronounced nonlinear “competition basin”. This behavior confirms that, at high modulation levels, the fourth-order nonlinear interaction term ($\Delta\nu_1^2\Delta\nu_2^2$) becomes dominant, progressively counteracting and suppressing the primary second-order signal contribution. To further isolate this interaction mechanism, Fig. 10(b) presents the signal evolution when the modulation depth of one channel is fixed at 4 mV while the other is systematically varied. The resulting parametric map clearly identifies the nonlinear "suppression boundary," demonstrating how the introduction of a secondary modulation component progressively degrades the fixed-channel signal response through inter-channel competition effects. Collectively, these multi-dimensional representations provide a comprehensive physical landscape of the nonlinear operating regime, enabling identification of

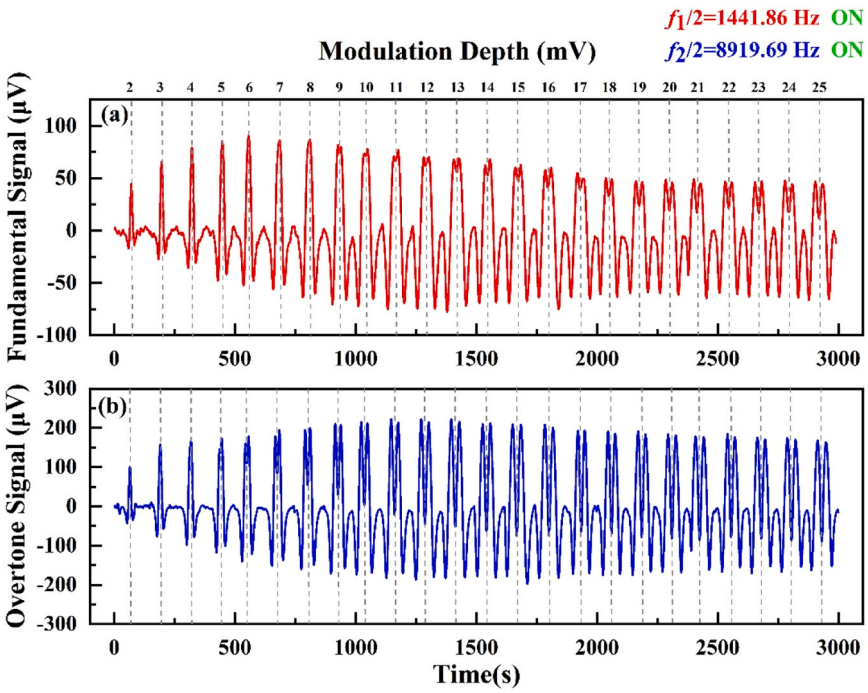

Fig. 7. Dual-channel signal evolution under equal-amplitude modulation ($m_1 = m_2$). (a) Fundamental and (b) overtone signal responses.

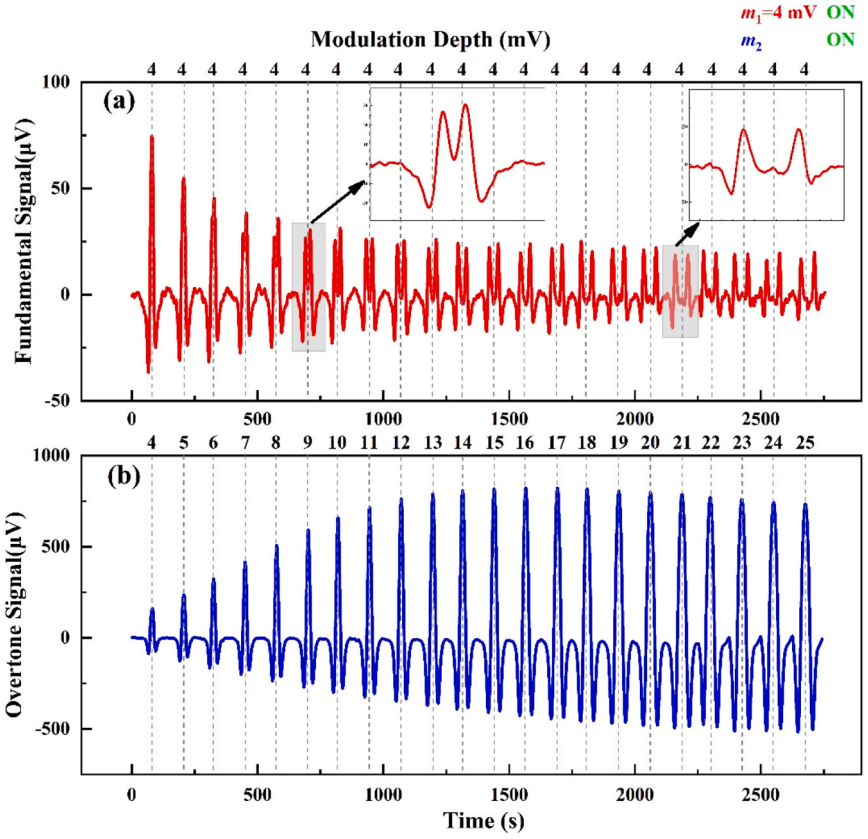

Fig. 8. Signal evolution under increasing overtone modulation depth. (a) The fundamental signal is fixed at $m_1 = 4$ mV, exhibiting severe cross-suppression and waveform splitting. (b) The overtone signal swept from $m_2 = 4$–25 mV.

the optimal operating conditions that preserve high sensitivity while avoiding deep nonlinear cancellation zones.

3.5. Smoothing effect of scanning rate on non-linear distortion

To investigate the influence of dynamic scanning on nonlinear waveform distortion, a modulation depth of 6 mV was intentionally

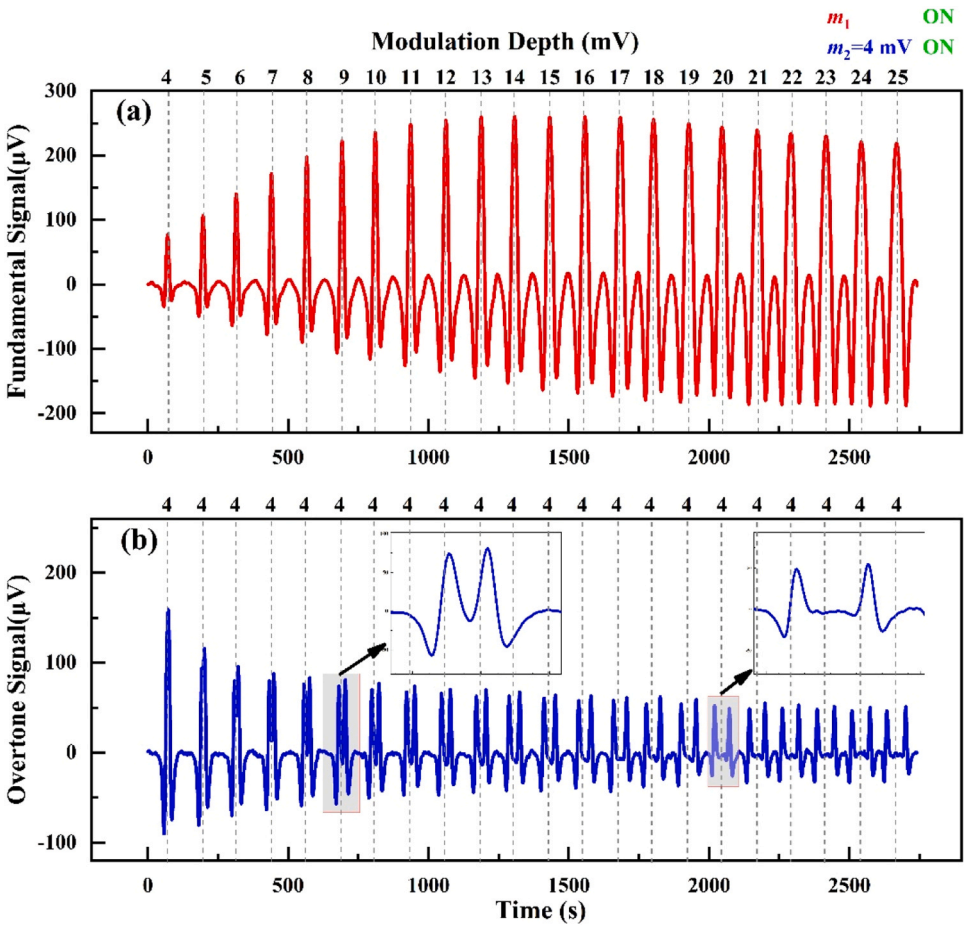

Fig. 9. Signal evolution under increasing fundamental modulation depth. (a) The fundamental signal swept from m_1 = 4–25 mV. (b) The overtone signal is fixed at m_2 = 4 mV, exhibiting severe cross-suppression and waveform splitting.

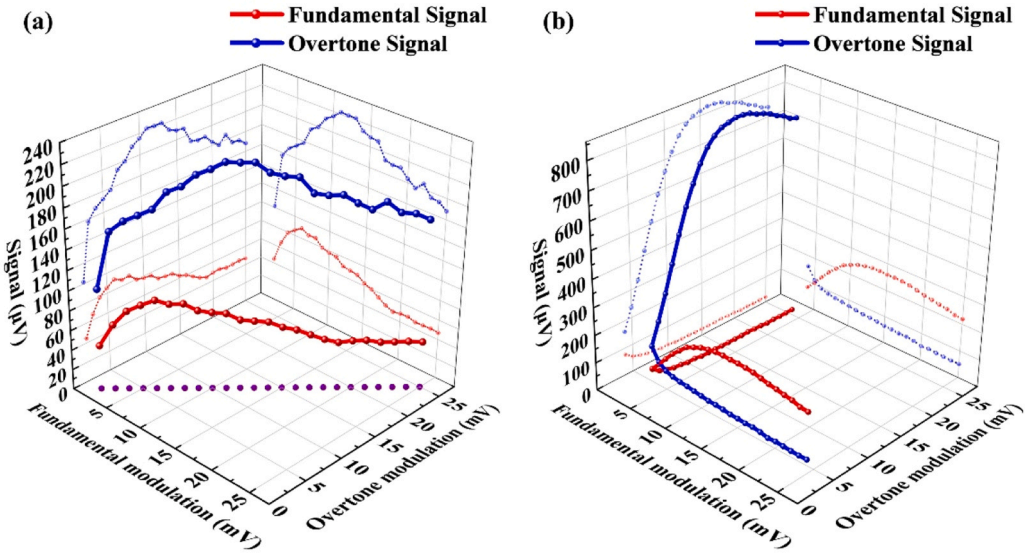

Fig. 10. Multi-dimensional parametric mapping of dual-channel signals revealing non-linear competition. (a) Signal evolution under synchronously increasing modulation depths (m_1 = m_2). (b) Signal mapping with one channel fixed at 4 mV while sweeping the other, explicitly defining the reciprocal cross-suppression boundaries.

selected as the baseline operating condition, as it corresponds to the onset of clearly observable nonlinear distortion. As shown in Fig. 11, at low scanning rates the waveform exhibits pronounced central dips and peak splitting, dominated by the *4-th* non-linear contribution, in agreement with the quasi-static theoretical model.

As the scanning rate increases, these high-frequency features are

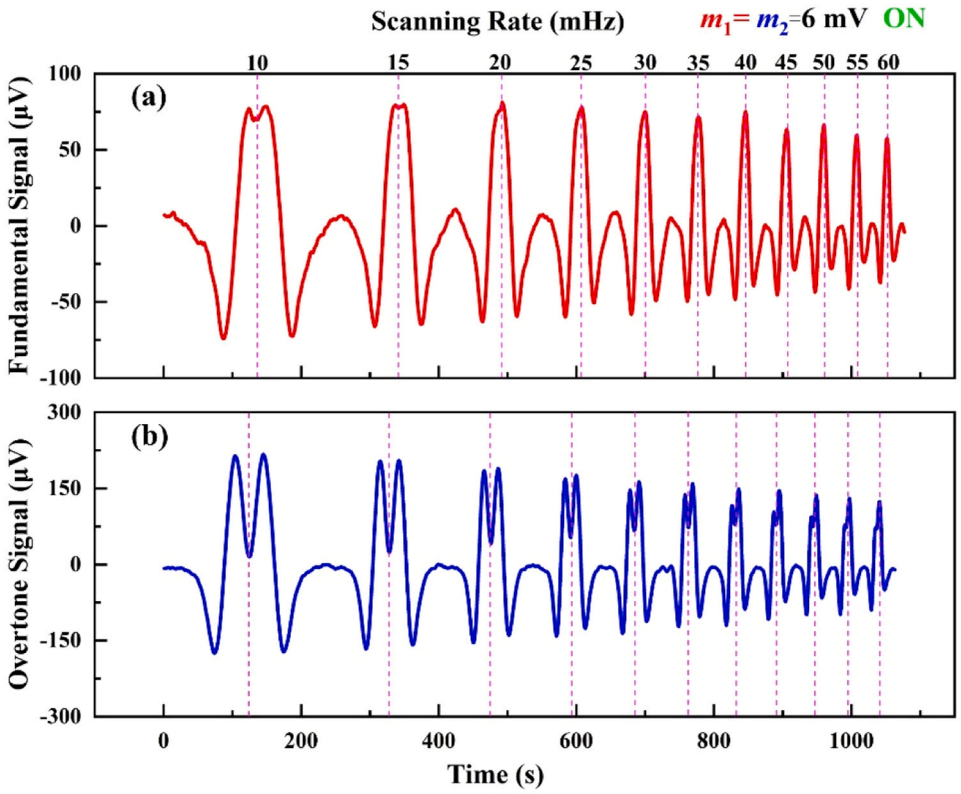

Fig. 11. Evolution of fundamental and overtone signals with increasing scanning rate at a constant modulation depth of 6 mV. (a) Evolution of Fundamental 2 *f* Signal. (b) Evolution of Overtone 2 *f* Signal.

progressively suppressed: the depth of the central dip decreases, and the waveform gradually evolves toward a quasi-Lorentzian single peak profile at higher rates. This behavior can be attributed to the low-pass filtering characteristics of the lock-in amplifier. From a signal-processing perspective, the measured time-domain signal corresponds to the convolution of the physical photoacoustic response with the impulse response of the LIA's, governed by its integration time constant τ. The fine structures associated with waveform splitting correspond to high-frequency components. With increasing scanning rate, the spectral features are mapped to higher temporal frequencies, causing the rapid signal variations in the non-linear region to exceed the effective bandwidth of the LIA. Consequently, these high-frequency distortion components are preferentially attenuated, leading to a smoothing of the waveform. By appropriately matching the scanning rate to the LIA integration time, non-linear distortion can be effectively suppressed while preserving sufficient modulation energy, thereby achieving an optimal balance between detection sensitivity and signal fidelity.

3.6. Frequency-domain mapping and synchronous extraction of adjacent spectral lines

While the previous sections focused on the time-domain characteristics of carrier suppression (Section 3.4) and waveform smoothing (Section 3.5), the proposed dual-frequency modulation scheme also provides enhanced capabilities for resolving overlapping spectral features in the frequency domain. To investigate this aspect, the frequency-domain response of the system under dual-modulation conditions was experimentally characterized.

Fig. 12 illustrates the dynamic mapping between the driving current, emitted wavenumber, and the corresponding detection envelope. Under typical operating conditions (~915 mbar), significant collisional broadening occurs, causing closely spaced absorption lines to merge into a broadened spectral profile. In conventional single-frequency WMS, this overlap leads to substantial cross-talk and reduced accuracy in concentration retrieval.

Fig. 12(a) and the magnified view in Fig. 12(b) present the frequency-domain characteristics under relatively low modulation depths (m_1 = 4 mV, m_2 = 9 mV). In this regime, the modulation amplitude is insufficient to achieve complete carrier suppression, resulting in a spectral envelope with a pronounced central component. This limitation is overcome by employing optimized modulation parameters (m_1 = 4 mV, m_2 = 21 mV). As shown in Figs. 12(c) and 12(d), when the laser driving current is linearly scanned from 95 mA to 103 mA, the increased modulation depth enhances the fourth-order nonlinear competition effect, promoting the redistribution of carrier energy into modulation sidebands. This process generates these quantifiable, high-energy frequency-domain sidebands to serve as "virtual probes".

The mapping results reveal distinct and independent trajectories for these probes in the wavenumber space: the fundamental dominated probe (purple trajectory) scans across the absorption region near 7306.5 cm^{-1}, while the first overtone-dominated probe (light blue trajectory) simultaneously addresses the adjacent absorption region near 7307.25 cm^{-1}.

Crucially, at a driving current of approximately 97 mA, these quantitative sideband probes coincide with the peak response regions of their absorption lines. This simultaneous multi-point targeting within a single scanning cycle demonstrates that the electrically generated sidebands can effectively isolate and synchronously interrogate overlapping spectral features, using a single optical path, thereby enabling efficient spectral discrimination in complex gas mixtures.

4. Conclusions

In this work, we proposed and experimentally validated a robust anti-interference QEPAS sensing technique based on single-laser dual-frequency superimposed modulation. By simultaneously injecting two

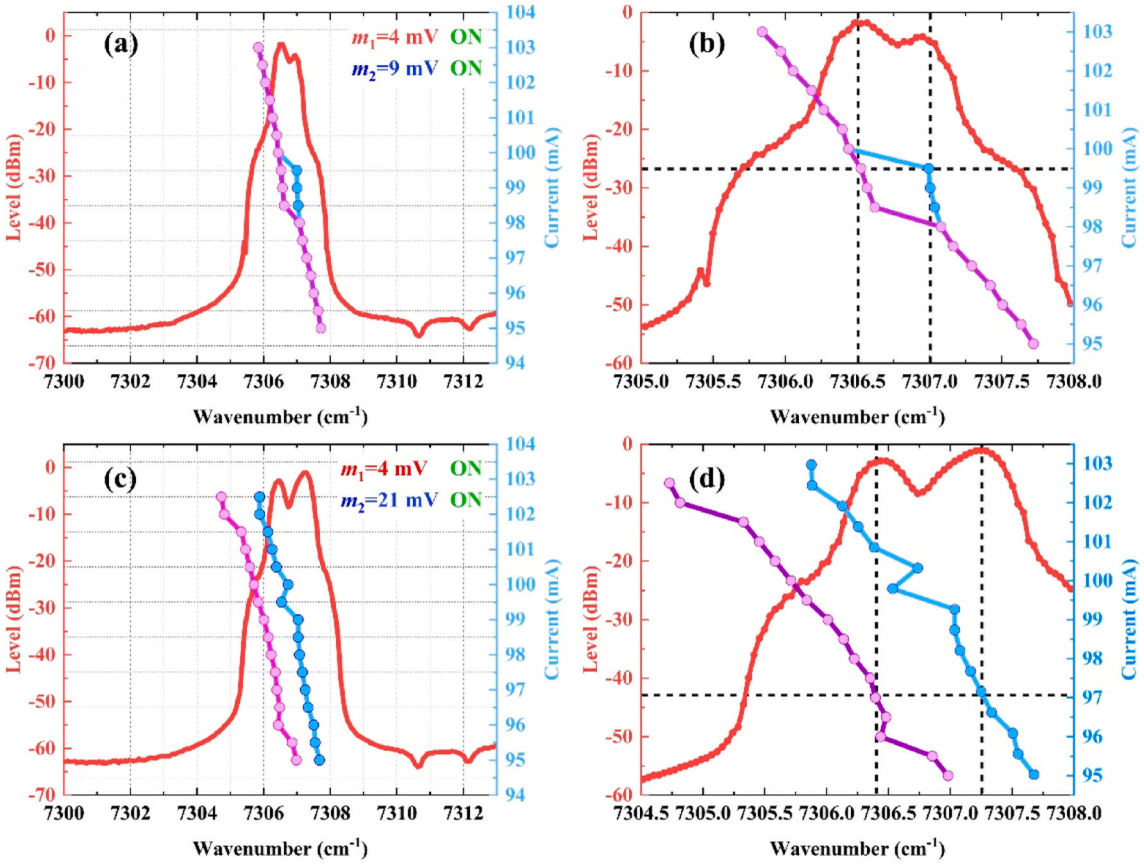

Fig. 12. Frequency-domain mapping of dual-frequency modulation probes and synchronous extraction of adjacent spectral lines. (a, b) Broad and continuous spectral envelope under insufficient modulation depth, where carrier suppression is incomplete. (c, d) Dynamic mapping between driving current (95–103 mA) and wavenumber space of the virtual probes (7306.5 cm^{-1} and 7307.25 cm^{-1}) under optimized dual-frequency modulation.

high-frequency sinusoidal signals matched to the fundamental and overtone modes of a QTF into a single DFB laser, dual-channel orthogonal demodulation was achieved within a compact and simplified optical architecture. Compared with conventional multi-laser schemes, the proposed approach eliminates beam-combining complexity, thereby enhancing system stability while significantly reducing size and cost.

A key contribution of this study is the development of a comprehensive physical model that incorporates both RAM and high-order nonlinear competition effects, providing a fundamental understanding of inter-channel crosstalk mechanisms. Both theoretical analysis and experimental results demonstrate that the fourth derivative term of the gas absorption line shape plays a dominant role in driving non-linear competition and signal distortion. To mitigate these effects, a waveform optimization strategy based on dynamic control of the scanning rates was introduced, leveraging the low-pass filtering characteristics of the lock-in amplifier to suppress high-frequency non-linear distortions.

Furthermore, frequency-domain analysis revealed an additional capability of the proposed method: by exploiting electrically generated sidebands as independent “virtual probes,” the system enables synchronous and selective extraction of closely spaced and overlapping spectral features within a single scanning cycle.

In summary, the proposed approach not only advances hardware integration and system simplicity but also addresses the fundamental challenge of non-linear interference in multi-frequency modulation. It establishes a solid theoretical and experimental foundation for the development of next-generation compact QEPAS sensors with enhanced sensitivity, robustness, and multi-dimensional detection capability, with promising applications in environmental monitoring, combustion diagnostics, and isotope analysis.

CRediT authorship contribution statement

Vincenzo Spagnolo: Writing – review & editing, Resources, Project administration, Conceptualization. **Hongpeng Wu:** Writing – review & editing, Supervision, Project administration, Data curation, Conceptualization. **Lei Dong:** Writing – review & editing, Supervision, Project administration, Conceptualization. **Pietro Patimisco:** Writing – review & editing, Conceptualization. **Angelo Sampaolo:** Writing – review & editing, Methodology, Investigation. **Marilena Giglio:** Writing – review & editing, Methodology. **Yan Gao:** Formal analysis, Conceptualization. **Chaofeng Sun:** Methodology, Investigation, Conceptualization. **Lei Yang:** Methodology, Investigation, Conceptualization. **Xiaowen Shen:** Writing – original draft, Methodology, Investigation, Conceptualization.

Declaration of Competing Interest

The authors declare that they have no known competing financial interests or personal relationships that could have appeared to influence the work reported in this paper.

The author is an Editorial Board Member/Editor-in-Chief/Associate Editor/Guest Editor for this journal and was not involved in the editorial review or the decision to publish this article.

Acknowledgments

This work was supported by Jing-Jin-Ji Regional Integrated Environmental Improvement-National Science and Technology Major Project of Ministry of Ecology and Environment of China (No. 2025ZD1200704); The National Natural Science Foundation of China (NSFC) (Nos. 62475137, 62235010, 62502163, 62501370); Shanxi

Provincial Special Fund for Scientific and Technological Cooperation and Exchange (Nos. 202404041101022, 202304041101019); Fundamental Research Program of Shanxi Province, China (No. 202403021212183, 202303021222034); The Scientific and Technological Innovation Programs of Higher Education Institutions in Shanxi Province of China (2024L014); National Engineering Research Center of UHV Technology and New Electrical Equipment Basis (Grant No. NERCUHE−2024-KF−12). Authors from Polysense Lab acknowledge funding from Project PNC 0000001 D3–4-Health Digital Driven Diagnostics, Prognostics and Therapeutics for sustainable Health Care (CUP: B83C22006120001) and MUR-Dipartimenti di Eccellenza 2023–2027-Quantum Sensing and Modelling for One-Health (QuaSiModO).

Data availability

Data will be made available on request.

References

[1] M. Gu, J. Chen, Y. Zhang, T. Tan, G. Wang, K. Liu, X. Gao, J. Mei, Portable TDLAS sensor for online monitoring of CO_2 and H_2O using a miniaturized multi-pass cell, Sensors 23 (4) (2023) 2072.
[2] Z. Li, Q. Zhang, Z. Wang, J. Dai, A highly sensitive low-pressure TDLAS sensor for detecting dissolved CO and CO_2 in transformer insulating oil, Opt. Laser Technol. 174 (2024) 10622.
[3] B. Li, G. Menduni, M. Giglio, P. Patimisco, A. Sampaolo, A. Zifarelli, H. Wu, V. Spagnolo, L. Dong, Quartz-enhanced photoacoustic spectroscopy (QEPAS) and beat frequency-QEPAS techniques for air pollutants detection: a comparison in terms of sensitivity and acquisition time, Photoacoustics 31 (2023) 100479.
[4] H. Ma, Y. Chen, S. Qiao, Y. He, Y. Ma, A high sensitive methane QEPAS sensor based on self-designed trapezoidal-head quartz tuning fork and high power diode laser, Photoacoustics 42 (2025) 100683.
[5] W. Ye, W. Liu, W. Luo, J. Xiao, L. He, Y. Huang, D. Zhu, Calibration-free near-infrared methane sensor system based on BF-QEPAS, Infrared Phys. Technol. 133 (2023) 104784.
[6] S. Qiao, X. Liu, Z. Lang, Y. He, W. Chen, Y. Ma, Quartz-enhanced laser spectroscopy sensing, Light. Sci. Appl. 15 (2026) 5.
[7] Y. Wang, S. Chen, Q. Kong, J. Gao, Research on CO concentration detection based on deep learning and TDLAS technology, Opt. Lasers Eng. 181 (2024) 108420.
[8] Y. Liu, Q. Shang, L. Chen, E. Wang, X. Huang, X. Pang, S. Li, Y. Lyu, Application of portable CH_4 detector based on TDLAS technology in natural gas purification plant, Atmosphere 14 (12) (2023) 1709.
[9] T. Liang, S. Qiao, Y. Chen, Y. He, Y. Ma, High-sensitivity methane detection based on QEPAS and H-QEPAS technologies combined with a self-designed 8.7 kHz quartz tuning fork, Photoacoustics 36 (2024) 100592.
[10] V. Zecchino, L. Lombardi, C. Marzocca, P. Patimisco, A. Sampaolo, V.L. Spagnolo, Development of compact electronics for QEPAS sensors, Sensors 25 (21) (2025) 6718.
[11] Y. Li, T. Zhang, G. Li, H. Zhang, P. Liu, C. Wang, C. Lou, Detection of exhaled methane in gastrointestinal disease population based on TDLAS, IEEE Sens. J. 24 (19) (2024) 31095–31103.
[12] Z. Li, D. Jiang, M. Zhang, J. Li, Diode laser absorption spectroscopy for real-time detection of breath oxygen, Infrared Phys. Technol. 133 (2023) 104815.
[13] İ. Bayrakli, Measuring and correlating the concentration levels of biomarkers in exhaled breath, Measurement 236 (2025) 119202.
[14] T. Seoudi, D. Ayache, O. Benabbad, F. Pages, J. Charensol, M. Bahriz, R. Valles, A. Vicet, Breath analysis by quartz enhanced photoacoustic spectroscopy: a clinical study, Field Laser Appl. Ind. Res. (FLAIR) (2024) (Sep 2024). ⟨https://hal.science/hal-04770606v1⟩ (Assise, Italy).
[15] F.A. Naoum, D. Ayache, T. Seoudi, D.A. Diaz-Thomas, A. Baranov, F. Pages, M. Bahriz, A. Vicet, Breath isoprene sensor based on quartz-enhanced photoacoustic spectroscopy, Sensors 25 (21) (2025) 6732.
[16] Z. Wang, Q. Wang, J.Y.L. Ching, J.C.Y. Wu, G. Zhang, W. Ren, A portable low-power QEPAS-based CO_2 isotope sensor using a fiber-coupled interband cascade laser, Sens. Actuators B Chem. 246 (2017) 710–715.
[17] M. Olivieri, A. Elefante, G. Menduni, M. Giglio, H. Wu, L. Dong, V.M.N. Passaro, A. Sampaolo, Simultaneous detection of $^{12}CH_4$, $^{13}CH_4$, and related isotope ratio exploiting a frequency-multiplexed mid-infrared quartz-enhanced photoacoustic sensor, ACS Sens. 11 (1) (2025) 247–256.
[18] M. Giglio, A. Sampaolo, P. Patimisco, D. Pinto, G. Menduni, A. Elefante, V.M. N. Passaro, V. Spagnolo, Quartz-enhanced photoacoustic spectroscopy of methane isotopologues, Photon. Instrum. Eng. VIII Proc. SPIE 11693 (2021) 52–57.
[19] V. Spagnolo, L. Dong, A.A. Kosterev, F.K. Tittel, Modulation cancellation method for isotope $^{18}O/^{16}O$ ratio measurements in water, Opt. Express 20 (3) (2012) 3401–3407.
[20] Z. Wang, Q. Wang, J.Y.L. Ching, J.C.Y. Wu, G. Zhang, W. Ren, A portable low-power QEPAS-based CO_2 isotope sensor using a fiber-coupled interband cascade laser, Sens. Actuators B Chem. 246 (2017) 710–715.
[21] W. Jin, N. Cao, Y. Ma, A highly sensitive TDLAS-based water vapor isotopes sensor using a quantum cascade laser, Sensors 25 (3) (2025) 840.
[22] B. Wang, X. Tang, Y. Gan, X. Li, Y. Lu, A TC/WMS-TDLAS mid-infrared detection method for ultra-low concentration carbon isotope methane, J. Anal. At. Spectrom. 37 (12) (2022) 2615–2624.
[23] W. Wu, L. Zhang, D. Zhu, Z. Shi, B. Jin, Spectroscopic techniques to analyze stable carbon isotopic compositions of carbon dioxide, methane and volatile organic compounds, J. Anal. At. Spectrom. 39 (6) (2024) 1444–1453.
[24] J.M. Supplee, E.A. Whittaker, W. Lenth, Theoretical description of frequency modulation and wavelength modulation spectroscopy, Appl. Opt. 33 (27) (1994) 6294–6302.
[25] A.L. Chakraborty, A. Roy, Wavelength modulation spectroscopy, in: D.K. Singh, M. Pradhan, A. Materny (Eds.), Modern Techniques of Spectroscopy. Progress in Optical Science and Photonics, Springer, Singapore, 2021, p. 13.
[26] S. Schilt, L. Thévenaz, Wavelength modulation photoacoustic spectroscopy: theoretical description and experimental results, Infrared Phys. Technol. 48 (2) (2006) 154–162.
[27] L. Qin, S. Bi, R. Chen, Y. Zhao, J. Shi, H. Zhang, Z. Wang, Two-component gas sensor of time-division multiplexing technique based on QEPAS and LITES, IEEE Photon. Technol. Lett. 36 (17) (2024) 1085–1088.
[28] H. Zhang, Y. Yu, S. Bi, Q. Zhang, C. Tian, Z. Wang, The intra-cavity QEPAS sensor using fiber-ring laser for C_2H_2 and CO_2 detection, Microw. Opt. Technol. Lett. 65 (11) (2023) 3021–3026.
[29] H. Xu, Y. Feng, Z. Chen, Z. Zhuang, J. Xia, Y. Zhao, S. Zhang, Dual-component beat-frequency quartz-enhanced photoacoustic spectroscopy gas detection system, Photonics 12 (8) (2025) 747.
[30] W. Ye, Z. Xia, L. Hu, W. Luo, W. Liu, X. Xu, C. Zheng, Infrared dual-gas CH_4/C_2H_2 sensor system based on dual-channel off-beam quartz-enhanced photoacoustic spectroscopy and time-division multiplexing technique, Spectrochim. Acta A 285 (2023) 121908.
[31] H. Zhang, S. Bi, J. Zhao, Y. Zhao, L. Qin, J. Shi, Dual-gas intra-cavity QEPAS sensor based on frequency division multiplexing using two acoustic microresonators, J. Light. Technol. 42 (14) (2024) 5033–5040.
[32] P. Patimisco, N. Ardito, E. De Toma, D. Burghart, V. Tigaev, M.A. Belkin, V. Spagnolo, Quartz-enhanced photoacoustic sensor based on a multi-laser source for in-sequence detection of NO_2, SO_2, and NH_3, Sensors 23 (21) (2023) 9005.
[33] R. De Palo, N. Ardito, A. Zifarelli, A. Sampaolo, M. Giglio, P. Patimisco, V. Spagnolo, Greenhouse gases detection exploiting a multi-wavelength interband cascade laser source in a quartz-enhanced photoacoustic sensor, Sensors 25 (8) (2025) 2442.
[34] R. Cui, H. Wu, F.K. Tittel, V. Spagnolo, W. Chen, L. Dong, Folded-optics-based quartz-enhanced photoacoustic and photothermal hybrid spectroscopy, Photoacoustics 35 (2024) 100580.
[35] S. Qiao, Y. He, H. Sun, P. Patimisco, A. Sampaolo, V. Spagnolo, Y. Ma, Ultra-highly sensitive dual gases detection based on photoacoustic spectroscopy by exploiting a long-wave, high-power, wide-tunable, single-longitudinal-mode solid-state laser, Light. Sci. Appl. 13 (2024) 100.
[36] S. Qiao, B. Liu, Z. Lv, Y. He, X. Zhi, L. Liu, A. Mandelis, Y. Ma, Elliptical acoustic resonator-based dual-Quartz-enhanced photoacoustic spectroscopy sensing, Anal. Chem. 98 (7) (2026) 5707–5714.
[37] Z. Lang, S. Qiao, T. Liang, Y. He, L. Qi, Y. Ma, Dual-frequency modulated heterodyne quartz-enhanced photoacoustic spectroscopy, Opt. Express 32 (1) (2024) 379–386.
[38] W. Liang, G. Wei, A. He, H. Shen, A novel wavelength modulation spectroscopy in TDLAS, Infrared Phys. Technol. 114 (2021) 103661.
[39] B. Deng, C. Sima, Y. Xiao, X. Wang, Y. Ai, T. Li, D. Liu, Modified laser scanning technique in wavelength modulation spectroscopy for advanced TDLAS gas sensing, Opt. Lasers Eng. 151 (2022) 106906.
[40] A. Sampaolo, P. Patimisco, M. Giglio, A. Zifarelli, H. Wu, L. Dong, V. Spagnolo, Quartz-enhanced photoacoustic spectroscopy for multi-gas detection: a review, Anal. Chim. Acta 1202 (2022) 339657.

Xiaowen Shen is now pursuing a Ph.D. degree in atomic and molecular physics at both the Institute of Laser Spectroscopy of Shanxi University, China and Polysense Lab at the Technical University of Bari, Italy. Her research is focused on the development of gas sensors, photoacoustic spectroscopy, photothermal spectroscopy and laser spectroscopy techniques.

Lei Yang received his Master degree in detection technology and automation device from Northwestern Polytechnical University, China, in 2015. Currently,he is a lecturer at the College of Physical and Electronic Sciences at Shanxi Datong University. His research interests include machine learning algorithms, fault diagnosis and other artificial intelligence fields.

Chaofeng Sun is now pursuing a Ph.D.degree in atomic and molecular physics in the Institute of Laser Spectroscopy of Shanxi University, China. His research has focused on the development of photoacoustic spectroscopy,photothermal spectroscopy and laser spectroscopy techniques.

Yan Gao received his Ph.D degree in optics from Shanxi University, China in 2015. He is an associate professor at Institute of intelligent Optoelectronics at Shanxi Datong University. His research interests encompass ultrafast optics, optical sensors and laser spectroscope techniques.

Marilena Giglio received her M.S. degree (cum laude) in applied physics in 2014 and her Ph.D. degree in physics in 2018 from the University of Bari. Since 2021, she has worked as an assistant professor at the Physics Department of the Technical University of Bari. Her research activity is focused on the development of gas sensors based on quartz enhanced photoacoustic spectroscopy and on the optical coupling of hollow-core waveguides with interband- and quantum-cascade lasers.

Angelo Sampaolo obtained his Master degree in Physics in 2013 and the Ph.D. Degree in Physics in 2017 from University of Bari. He was an associate researcher in the Laser Science Group at Rice University from 2014 to 2016 and associate researcher at Shanxi University since 2018. Starting from December 2026, he is Full Professor at Polytechnic of Bari. His research activity has included the study of the thermal properties of heterostructured devices via Raman spectroscopy. Most recently, his research interest has focused on the development of innovative techniques in trace gas sensing, based on Quartz-Enhanced Photoacoustic Spectroscopy and covering the full spectral range from near-IR to THz. His research activity is documented by more than 200 Scopus publications and 6 filed patents (more than 6400 citations, h-index 50).

Pietro Patimisco obtained the Master degree in Physics (cum laude) in 2009 and the Ph.D. Degree in Physics in 2013 from the University of Bari. Since 2023, he is Associate professor at the University of Bari. He was a visiting scientist in the Laser Science Group at Rice University in 2013 and 2014. Dr. Patimisco's scientific activity addressed both micro-probe optical characterization of semiconductor optoelectronic devices and optoacoustic gas sensors. Recently, his research activities included the study and applications of trace-gas sensors, such as quartz-enhanced photoacoustic spectroscopy and cavity enhanced absorption spectroscopy in the mid infrared and terahertz spectral region. His research activity is documented by more than 230 Scopus publications and 6 filed patents (more than 7400 citations, h-index 54).

Vincenzo Spagnolo obtained the Ph.D. in physics in 1994 from University of Bari. Since 2004, he works at the Technical University of Bari, formerly as assistant and associate professor and, starting from 2018, as full Professor of Physics. Since 2025, he director of the PhD School in Physics of the University of Bari. He is the director of the joint research lab Polysense between Technical University of Bari and THORLABS GmbH, fellow member of SPIE and senior member of OSA. His research interests include optoacoustic gas sensing and spectroscopic techniques for real-time monitoring. His research activity is documented by more than 350 publications and six filed patents. He has given more than 70 invited presentations at international conferences and workshops.

Lei Dong received his Ph.D. degree in optics from Shanxi University, China, in 2007. From June, 2008 to December, 2011, he worked as a post-doctoral fellow in the Electrical and Computer Engineering Department and Rice Quantum Institute, Rice University, Houston, USA. Currently he is a professor in the Institute of Laser Spectroscopy of Shanxi University. His research activities research activities are focused on research and development in laser spectroscopy, in particular photoacoustic spectroscopy applied to sensitive, selective and real-time trace gas detection, and laser applications in environmental monitoring, chemical analysis, industrial process control, and medical diagnostics. He has published more than 100 peer reviewed papers with $>$ 2200 positive citations.

Hongpeng Wu received his Ph.D. degree in atomic and molecular physics from Shanxi University, China, in 2017. From 2015–2016, he studied as a joint Ph.D. student in the electrical and computer engineering department and rice quantum institute, Rice University, Houston, USA. Currently he is a professor in the Institute of Laser Spectroscopy of Shanxi University. His research interests include optical sensors and laser spectroscopy techniques.